ACTA ONCOLOGICA, 2017
VOL. 56, NO. 11, 1437–1443
https://doi.org/10.1080/0284186X.2017.1350287

Taylor & Francis
Taylor & Francis Group

ORIGINAL ARTICLE



# Development of an interlaced-crossfiring geometry for proton grid therapy

Thomas Henry[a], Niels Bassler[a], Ana Ureba[a], Toshiro Tsubouchi[b], Alexander Valdman[c] and Albert Siegbahn[a]

[a]Medical Radiation Physics, Department of Physics, Stockholm University, Stockholm, Sweden; [b]Department of Radiation Oncology, Graduate School of Medicine, Osaka University, Osaka, Japan; [c]Department of Oncology and Pathology, Karolinska University Hospital, Stockholm, Sweden

**ABSTRACT**

**Background:** Grid therapy has in the past normally been performed with single field photon-beam grids. In this work, we evaluated a method to deliver grid therapy based on interlacing and crossfiring grids of mm-wide proton beamlets over a target volume, by Monte Carlo simulations.

**Material and methods:** Dose profiles for single mm-wide proton beamlets (1, 2 and 3 mm FWHM) in water were simulated with the Monte Carlo code TOPAS. Thereafter, grids of proton beamlets were directed toward a cubic target volume, located at the center of a water tank. The aim was to deliver a nearly homogeneous dose to the target, while creating high dose heterogeneity in the normal tissue, i.e., high gradients between valley and peak doses in the grids, down to the close vicinity of the target.

**Results:** The relative increase of the beam width with depth was largest for the smallest beams (+6.9 mm for 1 mm wide and 150 MeV proton beamlets). Satisfying dose coverage of the cubic target volume ($\sigma < \pm 5\%$) was obtained with the interlaced-crossfiring setup, while keeping the grid pattern of the dose distribution down to the target (valley-to-peak dose ratio <0.5 less than 1 cm before the target). Center-to-center distances around 7–8 mm between the beams were found to give the best compromise between target dose homogeneity and low peak doses outside of the target.

**Conclusions:** A nearly homogeneous dose distribution can be obtained in a target volume by crossfiring grids of mm-wide proton-beamlets, while maintaining the grid pattern of the dose distribution at large depths in the normal tissue, close to the target volume. We expect that the use of this method will increase the tumor control probability and improve the normal tissue sparing in grid therapy.

**ARTICLE HISTORY**
Received 1 May 2017
Accepted 21 June 2017

## Introduction

Grid therapy (or spatially fractionated radiation therapy), evolved from the observation that some tissues have an increased tolerance to radiation, when the irradiated volume is decreased [1–3]. This is known as the dose-volume effect and has been studied for organs such as the skin and the spinal cord [1,4].

Today, grid therapy with megavoltage X-ray beams is used at a few clinics around the world mainly to shrink bulky tumors and provide palliative care when other treatment options have been exhausted [5–7]. The size of the beamlets, building up the grid in these treatments, is in the order of 1 $cm^2$ and the target is typically irradiated from a single direction. The dose distribution constitutes of high doses (peaks) and low doses (valleys) and this pattern is present in the normal tissue but also in the targeted volume, leaving parts of it completely unirradiated. This poses an extra challenge to determine the tumor control of such highly heterogeneous dose distributions and therefore questions the curative value of grid therapy as it used now clinically.

To maximally exploit the dose-volume effect, experiments with photon microbeams have also been conducted in the last decades with either single grid irradiation [8,9] or interlacing of the microbeam grids from two orthogonal directions [10,11]. However, the technical implementation of photon microbeams requires the use of highly collimated synchrotron radiation which are not widely available, less so for clinical applications. As an intermediate step between grid therapy with microbeams and with larger cm-wide beams, grid therapy with beamlets of widths in the interval 0.3–0.7 mm (a.k.a. minibeams) has also been proposed [10]. Research related to minibeam therapy with proton and ion beamlets has also been studied, exploiting the limited range of these charged particles to better spare sensitive structures located behind the target volume [12,13].

In previous studies [14,15], a new experimental grid therapy method based on crossfiring of interlaced proton grids has been suggested. With this method, homogeneous doses could be delivered in the targeted volumes. In Henry et al. [14], a strong emphasis was put on retaining the grid pattern of the dose distribution in the surrounding normal tissues, from the skin down to the close vicinity of the target, to potentially reduce the side-effects of such experimental treatments. This new method was suggested with the use of

CONTACT Thomas Henry thomas.henry@fysik.su.se Medical Radiation Physics, Department of Physics, Stockholm University, Karolinska University Hospital Solna, Heliport (P9:02), Box 260 S-17176, Stockholm, Sweden

Supplemental data for this article can be accessed here.

clinically available beam sizes, which could provide a technically feasible solution which can readily be applied at existing proton therapy centers.

In this work the main aim was: 1) to evaluate if the same interlaced-crossfiring method could be applied with smaller, mm-wide proton beams, with the same dose objectives in a simple irradiation case (homogeneous target dose, highly heterogeneous normal tissue dose), and 2) to compare different sets of grid parameters (see below) and find which combinations would provide the most clinically desirable dose distributions.

This study was divided in two parts. In the first part, dose distributions produced by single monoenergetic and mm-wide (full-width at half maximum, FWHM) beamlets were determined with Monte-Carlo simulations to quantitatively investigate how such small beamlets scatter in a given medium and how the Bragg peak dose is reduced at larger depths. In the second part of this study, simulation results for single beamlets were used to calculate the dose distributions produced by proton grids. Simulation of a simple grid irradiation of a small target volume at the center of a water tank was performed. Several irradiation geometries, using multiple irradiation angles and grid parameters, were studied.

## Material and methods

### Grid parameters

For this study, four additional parameters to those known from conventional therapy have been considered to quantify and evaluate grid therapy: (1) the center-to-center (c-t-c) distance parameter specifies the distance between the individual beamlets making up the grid. (2) The initial beamlet width parameter is of importance as it may influence the tissue tolerance and depth at which the beamlets will begin to overlap. (3) The quality of the grid is here described as the valley-to-peak dose ratio (VPDR) variable, which is a quantity that reaches zero for a perfect grid with zero dose in the valley. Vice versa, the VPDR reaches 1 if the dose is homogenous. The ideal scenario which can be used as an optimization objective, is thus to achieve a VPDR of 0 outside the tumor and 1 inside it. In most publication on grid therapy the inverse parameter (the PVDR) is mentioned to characterize the heterogeneity of the dose distribution produced in beam grids. We will not use the PVDR term, since it is divergent when the valley dose reaches zero, possibly leading to numerical unstable conditions e.g., during optimization. (4) Finally, the peak-dose variable deserves special attention in grid therapy. Dose is a point-quantity, and we regard average dose as a less meaningful descriptor when VPDRs are not equal to 1 (i.e., a grid is present). The peak-dose in the grid is reported together with the VPDR parameter. This poses an extra challenge to Monte Carlo simulations to ensure a sufficiently small scoring volume, so the peak dose is properly recorded.

These four parameters and variables are not independent of each other, as the choice of c-t-c distance and initial beamlet size influences the achieved VPDR and peak dose.

### Monte carlo simulation parameters

The MC simulations were performed with the Geant4-based MC-code TOPAS [16] version 3.0.p1. The proton-beam transport was simulated in a water phantom. The G4_WATER component was used with a 75 eV mean excitation energy. The initial divergence of the proton beamlets was neglected as it was proven to have a limited impact on the lateral dose spreading in water compared to multiple Coulomb scattering [17]. The Gaussian primary proton kinetic energy spread was assumed to be 0.75% of the incident energy. Each monoenergetic beamlet had a circular Gaussian shape and a total of $5 \times 10^7$ histories were simulated. For all other parameters, the default TOPAS settings were used. The numerical stability of the peak doses was checked by varying the scoring grid dimensions.

### Single beamlet distributions

Dose distributions for single proton beamlets of 1, 2 and 3 mm initial widths (FWHM, defined at phantom surface) were simulated for five different energies: 70, 110, 150, 190 and 230 MeV, covering the energy range available at typical proton therapy facilities. Additionally, in order to relate to previous minibeam research [12,13], a 0.5 mm-wide beamlet (FWHM) was studied, for the same energy range. The geometry used was a $200 \times 200 \times 400\,mm^3$ water phantom. The dose to the medium was scored in a $50 \times 0.1 \times 400\,mm^3$ slice which was then binned to contain $0.1 \times 0.1 \times 0.5\,mm^3$ voxels. The MC transport cutoff range was set to 0.02 mm.

Depth-dose curves and transversal dose profiles were then determined for the simulated beamlets. The depth-dose profiles were normalized to the Gaussian peak dose at the phantom surface. The variation of the beamlet FWHMs with depth was determined from the transversal dose profiles.

### Irradiation with grids

Grids of proton beamlets were directed toward a $20 \times 20 \times 20\,mm^3$ cubic-shaped target, which was located at the center of a $200 \times 200 \times 200\,mm^3$ water phantom, with a spread-out Bragg peak (SOBP) (112–124 MeV). The water phantom was binned to obtain $0.2 \times 0.2 \times 0.2\,mm^3$ voxels and the MC transport cutoff range was set to 0.04 mm.

Grids containing beamlets with initial beam width of 1, 2 and 3 mm (FWHM) were chosen for the grid irradiations. Two types of grids were considered: 1) a 1-D grid made of elongated beamlets, spatially fractionated along one direction (Figure 1(a)) and 2) a 2-D grid made of circular (Gaussian) beamlets, spatially fractionated in two directions (Figure 1(b)). For the 1-D grid, 'beamlet width' refers to the width of the narrow side of the elongated beamlets. These elongated beamlets were created by superposing multiple circular, Gaussian beamlets. A total of 3 irradiation geometries were evaluated: 1) single grid irradiation from one direction, 2) two opposing interlacing grids (Figure 1(c)) and 3) four ($2 \times 2$ opposing, see Figure 2 in Henry et al. [14]) interlacing grids. Each of these geometries was evaluated with either 1-D grids or 2-D grids.

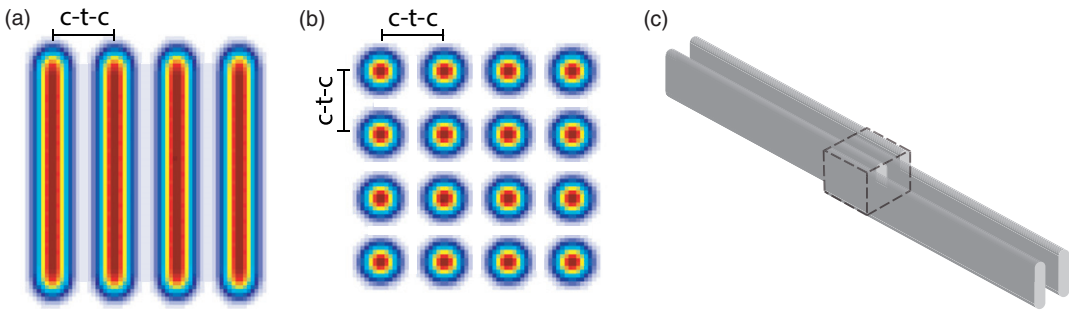


**Figure 1.** (a) A 1-D grid with 4 beamlets and (b) a 2-D grid with 16 beamlets. (c) 3-D illustration of two 1-D grids interlacing in a cubic target, each grid containing two elongated beamlets.

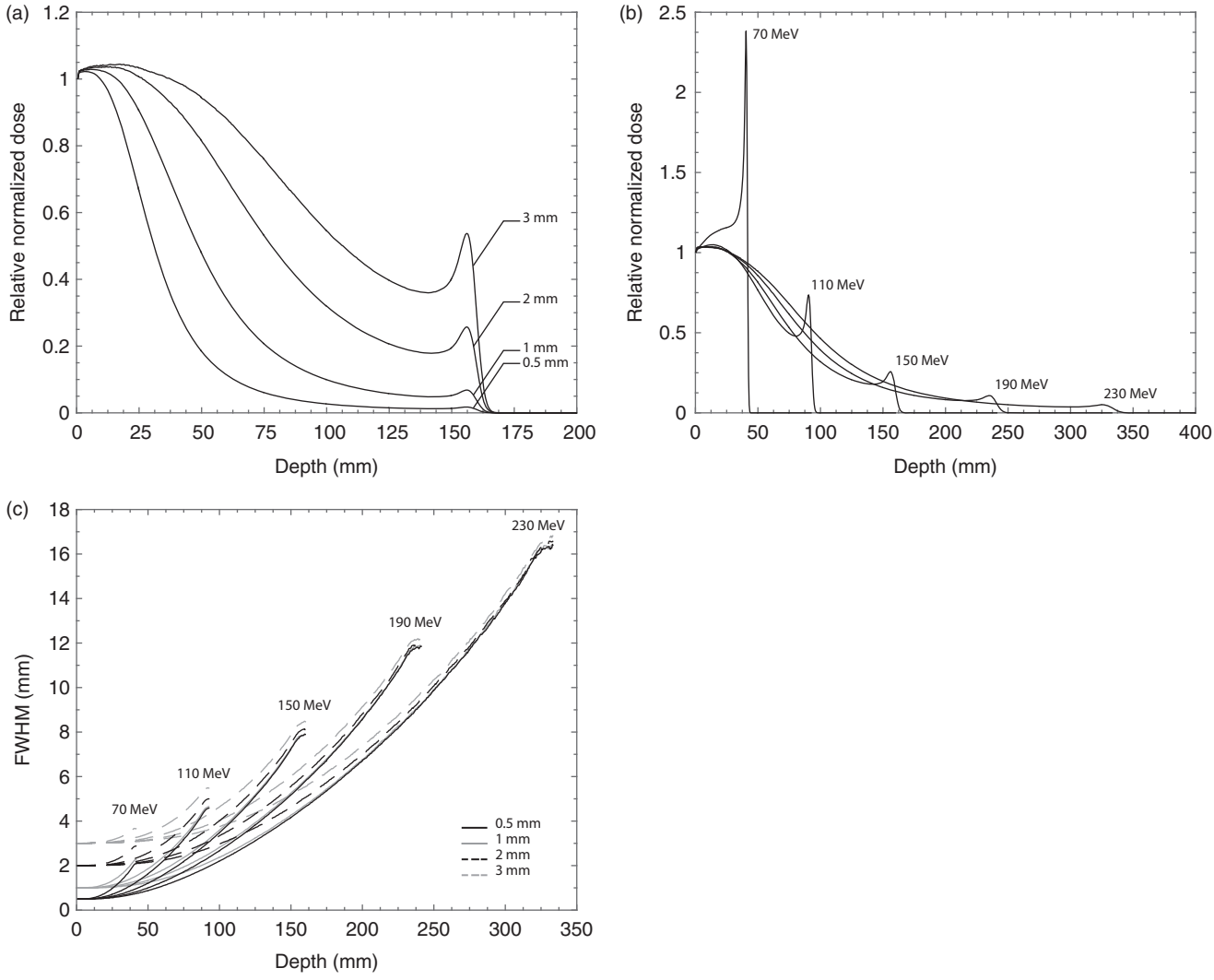


**Figure 2.** (a) Depth-dose profiles for proton beamlets of energy 150 MeV for four different initial beamlet FWHMs (0.5–3 mm), (b) Depth-dose profiles for 2 mm-wide beamlets (FWHM) for five different energies (70, 110, 150, 190, and 230 MeV), (c) Evolution of the beamlet width (FWHM) with depth for the four initial beamlet widths and five energies studied.

The dose distributions produced by the irradiation grids were then calculated by adding the simulated dose distributions for single proton beamlets, separated with the specified c-t-c distance. Different c-t-c distances inside the grids were used to evaluate the impact of this parameter on the resulting dose distributions inside and outside the target. Due to the simple geometry of the phantom, the target, and its symmetry, no optimization code was required: all SOBPs were equally-weighted for each irradiation setup.

### *Dose evaluation and grid parameter selection criteria*

To evaluate the relative dose distributions produced by the grid irradiations, the minimum and maximum doses given to 95% of the target volume were compared for different c-t-c distances and initial beamlet FWHMs. The peak doses and the VPDRs outside of the target volume were also determined at several depths (at entrance and at 1 and 2 cm distance (upstream) from the target). The overall normalization

Table 1. Dosimetric values obtained for single 1-D and single 2-D grid irradiations of a cubic target volume with 1, 2 and 3 mm-wide beamlets (FWHM). the dose was normalized (100%) to the mean target dose.

| | | | At phantom entrance | | 2 cm before target | | 1 cm before target | | Target coverage V (95%) | | |
|---|---|---|---|---|---|---|---|---|---|---|---|
| Beamlet size (FWHM) | C-t-c distance | Grid type | VPDR | Peak dose (%) | VPDR | Peak dose (%) | VPDR | Peak dose (%) | Min dose (%) | Max dose (%) | $\sigma$ (± %) |
| 1 mm | 3 mm | Single 1-D grid | 0.008 | 115 | 0.83 | 70 | 0.95 | 74 | 91 | 105 | 3.6 |
| | | Single 2-D grid | 0.004 | 309 | 0.82 | 77 | 0.96 | 76 | 91 | 105 | 3.6 |
| 2 mm | 4 mm | Single 1-D grid | 0.13 | 77 | 0.71 | 75 | 0.86 | 78 | 91 | 105 | 3.8 |
| | | Single 2-D grid | 0.13 | 142 | 0.70 | 87 | 0.87 | 83 | 91 | 105 | 3.5 |
| 3 mm | 5 mm | Single 1-D grid | 0.29 | 66 | 0.68 | 77 | 0.79 | 82 | 89 | 107 | 4.9 |
| | | Single 2-D grid | 0.30 | 100 | 0.67 | 91 | 0.79 | 90 | 90 | 107 | 4.7 |

of the dose was done relative to the mean target dose (100%).

The following criteria were applied in order to select a combination of the c-t-c distances and initial beamlet size which could be considered suitable for grid therapy: 1) The standard deviation of the target dose distribution should not exceed $\sigma = \pm 5\%$. 2) The peak dose in the normal tissue close to the target (2 cm before) should not exceed the mean target dose (100%). 3) For the irradiation geometries which were based on interlaced-crossfiring, the VPDR should not exceed 0.5 in the close vicinity of the target (1 cm before). The choice of 0.5 is arbitrary, and can be updated as radiobiological evidence is gathered. Thus, for given target doses and tissue type, acceptable VPDR and peak dose thresholds which produce a sufficient normal tissue sparing must be established. Here, only cases that would produce a peak dose that is at least twice as high as the valley dose close to the target were selected.

## Results

### Single beamlet distributions

The central axis dose decreased rapidly with depth, resulting in a Bragg peak which was lower than the entrance dose (Figure 2(a)). This effect is particularly noticeable for the smallest beamlet widths studied. When normalizing the entrance dose, the relative dose in the Bragg peak was 0.54 for the 3 mm-wide beamlet, but only 0.02 for the 0.5 mm-wide beamlet.

The reduction of the Bragg peak dose can also be observed in Figure 2(b) in which the central-axis depth-dose distributions for 2 mm-wide beamlets with energies of 70–230 MeV are shown. For a fixed initial beamlet width, the relative dose at the Bragg peak decreased with increasing initial proton energy, 2.4 for 70 MeV protons, down to 0.05 for 230 MeV protons.

The increase of the FWHM with depth, for an initial proton energy of 150 MeV, was larger for the narrowest beamlets: e.g.,+7.4 mm,+6.9 mm,+6.2 mm and +5.6 mm at the Bragg Peak for 0.5, 1, 2 and 3 mm-wide beamlets, respectively (Figure 2(c)). For mid-range to high energies, the FWHMs at the Bragg peak were very similar, independently of the initial beamlet size. The FWHM of the 0.5 mm beamlet was only 0.6 mm, 0.4 mm and 0.3 mm smaller compared to the 3 mm beamlet at the Bragg peak for 150, 190 and 230 MeV, respectively.

### Irradiation with grids

A preliminary study showed that the geometry with the two opposing 2-D grids produced a target dose distribution with numerous hot and cold spots, and an inferior dose homogeneity (> ± 30%), unless the c-t-c distance between the beamlets was greatly reduced, leading to high VPDRs already at the tank entrance. This geometry was therefore disregarded for this study.

For the other geometries studied, several trends can be observed: 1) When a single 1-D grid or a single 2-D grid is used, the VPDRs were high (>0.70) more than 2 cm upstream from the target. 2) When using the interlaced-crossfiring setups, a large c-t-c distance resulted in greatly increased normal-tissue peak-doses, relative to the target doses, independently of the initial beamlet width used, but also in a lower VPDR at all depths. A smaller c-t-c distance, inversely, resulted in a reduced normal tissue peak-dose relative to the target dose, and an increased valley dose in depth, leading to a higher VPDR. 3) The 2 × 2 opposing 1-D grids produced the lowest normal tissue peak-doses, while the 2 × 2 opposing 2-D grids produced the highest, especially at entrance. 4) For all cases, the target dose coverage fulfilled, or was very close to fulfill, the conventional homogeneous dose requirement, defined as 95% of the volume receiving 95–107% of the dose.

All data for selected beamlet widths, c-t-c distances and grid geometries are summarized in Tables 1–2 and Supplementary Tables 1–2. Smoothing or denoising techniques were not applied to the MC calculated dose distributions.

With 2 × 2 opposing and interlaced 1-D grids, with 2 mm-wide beamlets and a c-t-c distance of 8 mm, the target dose ranged from 93 to 105% with a standard deviation $\sigma = \pm 3.1\%$, while the normal tissue peak dose was kept below 37% from entrance down to the close vicinity of the target (Figure 3). The VPDR was 0.002 at entrance and 0.18 at 1 cm distance from the target.

Comparison of lateral dose distributions of the same interlaced-crossfiring geometry (2 × 2 opposing 1-D grids, 2 mm beamlets, 8 mm c-t-c) and a single grid geometry (1-D grid, 2 mm beamlets, 4 mm c-t-c) showed that similar target dose coverage could be achieved with these two setups (Figure 4(a,b)). The lateral profile inside the target was taken at the center of the target.

With interlaced-crossfiring grids of the target volume, the peak-doses were more than halved at all depths. Similarly,

**Table 2.** Dosimetric values obtained for different proton grid irradiations of a cubic target volume with 2 mm-wide beamlets (FWHM) and four different center-to-center distances. The dose was normalized (100%) to the mean target dose.

| | | | At phantom entrance | | 2 cm before target | | 1 cm before target | | Target coverage V (95%) | | |
|---|---|---|---|---|---|---|---|---|---|---|---|
| Beamlet size (FWHM) | C-t-c distance | Grid type | VPDR | Peak dose (%) | VPDR | Peak dose (%) | VPDR | Peak dose (%) | Min dose (%) | Max dose (%) | $\sigma$ (± %) |
| 2 mm | 6 mm | 2 opposing 1-D grids | 0.007 | 56 | 0.23 | 51 | 0.38 | 49 | 88 | 107 | 4.6 |
| | | 2 × 2 opposing 1-D grids | 0.007 | 28 | 0.24 | 25 | 0.41 | 26 | 89 | 105 | 3.9 |
| | | 2 × 2 opposing 2-D grids | 0.005 | 78 | 0.21 | 44 | 0.38 | 38 | 93 | 105 | 2.9 |
| | 7 mm | 2 opposing 1-D grids | 0.003 | 65 | 0.13 | 58 | 0.23 | 56 | 88 | 108 | 4.8 |
| | | 2 × 2 opposing 1-D grids | 0.003 | 33 | 0.13 | 29 | 0.26 | 29 | 89 | 106 | 4.1 |
| | | 2 × 2 opposing 2-D grids | 0.001 | 105 | 0.10 | 58 | 0.22 | 49 | 93 | 106 | 3.3 |
| | 8 mm | 2 opposing 1-D grids | 0.002 | 74 | 0.08 | 66 | 0.15 | 64 | 92 | 108 | 3.9 |
| | | 2 × 2 opposing 1-D grids | 0.002 | 37 | 0.08 | 33 | 0.18 | 33 | 93 | 105 | 3.1 |
| | | 2 × 2 opposing 2-D grids | 0 | 137 | 0.05 | 76 | 0.13 | 64 | 93 | 108 | 3.5 |
| | 9 mm | 2 opposing 1-D grids | 0.001 | 84 | 0.05 | 75 | 0.09 | 72 | 88 | 109 | 5.0 |
| | | 2 × 2 opposing 1-D grids | 0.001 | 42 | 0.05 | 37 | 0.12 | 37 | 89 | 106 | 4.2 |
| | | 2 × 2 opposing 2-D grids | 0 | 174 | 0.03 | 96 | 0.08 | 80 | 93 | 110 | 4.5 |

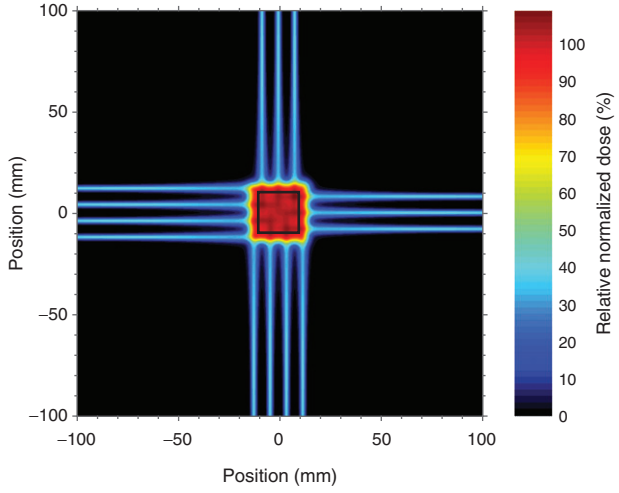


**Figure 3.** 2D dose distribution produced by irradiation of a cubic target with 2 × 2 opposing and interlaced 1-D grids with 2 mm-wide beamlets (FWHM) and a c-t-c distance of 8 mm.

the VPDRs at entrance, 2 and 1 cm before the target, were 0.13, 0.71 and 0.86 for the single 1-D grid irradiation and 0.002, 0.08, 0.18 for the 2 × 2 opposing 1-D grid geometry, respectively.

With the interlaced-crossfiring geometries, the VPDRs could be kept low (<0.2) from phantom surface to the vicinity of the target (Figure 5). With the single 1-D and 2-D grid irradiations, the VPDRs were above 0.5 already 3 cm before the target. A new variable to determine the quality of the dose distribution produced by the grid irradiation can be defined: The $d_{VPDR\gamma}$ describes at which depth the VPDR reaches $\gamma$ %. For the cases presented in Figure 5, $d_{VPDR50}$ was around 5.9 cm for the single grid irradiations, and 8.5 cm for the interlaced-crossfiring irradiations. As an optimization objective, we would like to maximize $d_{VPDR\gamma}$ for all $\gamma$.

## Discussion

Different grid irradiations of a cubic target volume were simulated, using the 3 proposed initial beamlet widths (1, 2 and 3 mm FWHM). The beam grids were interlaced and crossfired over the target volume to produce the desired level of dose homogeneity. The tumor-control probability is generally considered to be determined by the minimum target dose [18] and therefore, the production of a high minimum dose within the target volume was given a high priority. Outside the tumor, the grid structure of the dose distribution was preserved down to tissue depths close to the target volume.

Historically, grid therapy has been used with unidirectional grids. In clinical setups for palliative care and experimental setups using mini- and microbeams, the target is given very heterogeneous doses, with parts of it receiving high doses and parts of it left completely unirradiated. The clinical implications of these very heterogeneous dose distributions on the tumor control for curative treatments, independently of the beam widths, are still to be investigated. When a target dose homogeneity is attempted using only one irradiation grid, our work demonstrates that the grid pattern is lost already several centimeters before the target. Indeed in this case, the c-t-c distance has to be set to a value that leads to the overlapping of the beamlets in depth before the target, due to multiple Coulomb scattering occurring in the medium. As a consequence, high and nearly homogeneous doses are being delivered outside of the target, i.e., in the normal tissue.

However, the use of interlaced-crossfiring grids of protons with mm-wide beams, studied in this work, makes it possible to irradiate the normal tissue with relatively low doses, compared to the mean target dose (up to 3 times lower, depending on the geometry used and the depth), while keeping a homogeneous dose inside the target. The doses given to the normal tissue with this method is comparable with the doses delivered in conventional proton therapy treatments, but confined to relatively small volumes. Theoretically, this should result in an improved normal-tissue tolerance for many early and late responding organs. Also, delivering a homogenous dose to the target overcomes the problem of the unknown TCP inside this latter, reducing the number of unknown parameters in grid therapy, and therefore bringing this method closer to clinical applications for curative purposes.

The choice of initial beamlet widths for this work was based on the subsequent considerations: (1) The initial beamlet widths should be easier to produce at existing proton facilities than e.g., microbeams. Collimation for ion

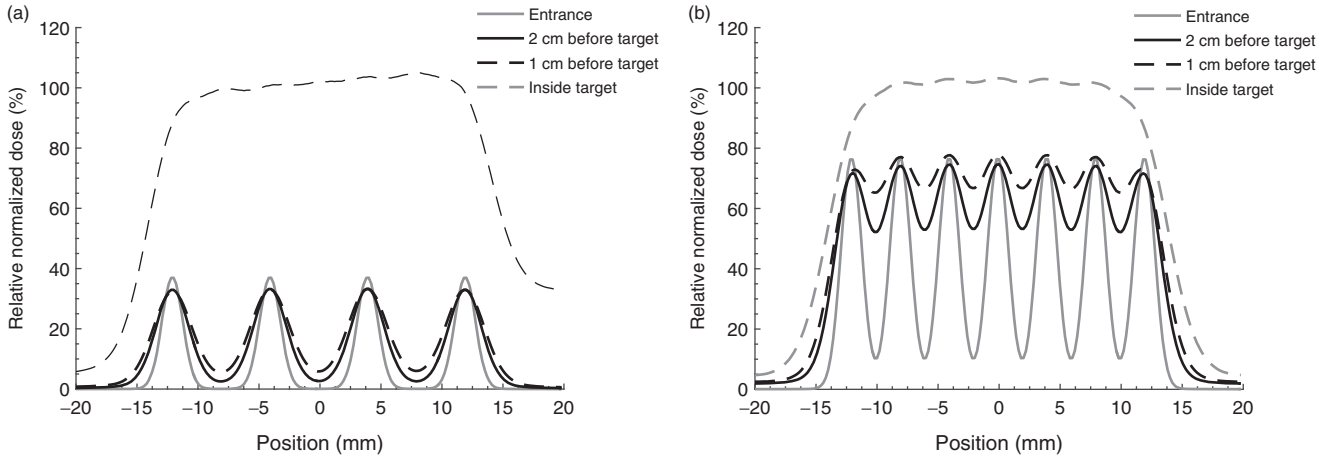


**Figure 4.** Comparison of lateral dose distributions at different depths obtained with: (a) 2 × 2 opposing 1-D grids with 2 mm-wide beamlets (FWHM) and a c-t-c distance of 8 mm, (b) a single 1-D grid with 2 mm-wide beamlets (FWHM) and a c-t-c distance of 4 mm. Both figures were normalized (100%) to the mean target dose.

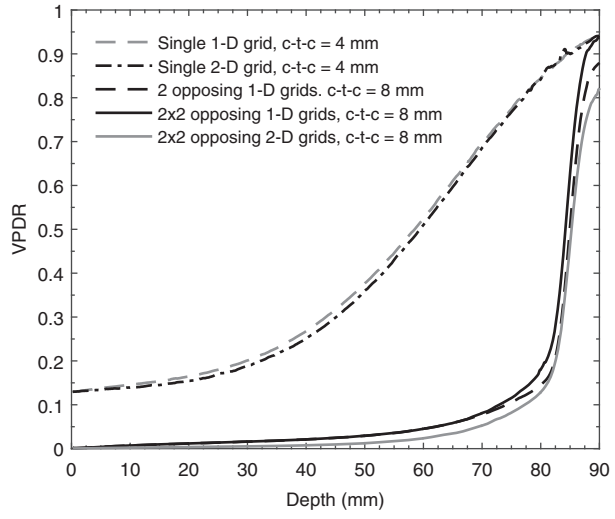


**Figure 5.** Evolution of the VPDR with depth in the normal tissue, from the entrance to the target volume, for 5 different grid irradiation geometries with 2 mm-wide beamlets (FWHM).

minibeams (0.3 mm) have already been successfully experimented [19]. We then expect the collimation of 1, 2 and 3 mm wide proton beamlets to be carried out with practical ease. (2) Rather than e.g., producing microbeams, where almost the entire broad beam is lost in the collimator, producing millimeter beamlets implies less loss of the primary beam in the collimator. This leads to a higher possible dose-rate in the target volume, less neutron production in the collimator and less activation of the collimator material. The treatment time will still remain higher than if conventional proton therapy was delivered though, and may impact collimator design. (3) The initial beamlet widths should not be smaller than the typical target setup error and beam-delivery accuracy that can be expected at a modern proton therapy center when motion mitigation techniques, such as stereotactic frames or high-frequency jet ventilation is used [20,21]. Hence, we conclude that the interlaced-crossfiring method is feasible at current proton therapy centers. (4) Finally, to our knowledge, the initial beamlet widths investigated in this work have not been studied so far for grid therapy.

The grid parameters, most notably the c-t-c distance had a very important impact on the final result. For the grid irradiations containing 2 or 3 mm-wide beamlets, a c-t-c distance of 8 mm seems suitable, because it resulted in a close to homogeneous dose distribution inside the cubic target, while keeping the VPDR and the peak doses in the normal tissue relatively low. For grids with 1 mm-wide beamlets and a c-t-c distance of 8 mm, the in-depth peak doses, VPDR and target dose coverage were acceptable but the entrance peak dose was very high (e.g., 527% for the 2 × 2 opposing 2-D grids geometry). Hence, a c-t-c distance of 7 or 6 mm or the use of another grid geometry (e.g., the 2 × 2 opposing 1-D grids geometry) might be more appropriate in order to reduce the entrance peak dose.

Which interlaced-crossfiring grid geometry that is the best is still subject to discussion. As discussed previously, the two opposing 2-D grid geometry is not recommended, as it does not allow a good dose coverage of the target without greatly compromising our dose objectives outside of it. With the interlaced 1-D grids, the spatial fractionation inside the grids is only one dimensional, reducing the risk for potential setup errors compared to the 2-D grids. When the irradiation geometries based on two opposing 1-D grid or 2 × 2 opposing 2-D grids are used, each voxel inside the target is mainly irradiated with a single beamlet, with only minor contributions from the neighboring beamlets. However, with the 2 × 2 opposing 1-D grid geometry, the entire target volume is irradiated by at least two perpendicular beamlets. This is of relevance for the treatment robustness which should be taken into consideration. Indeed, the misalignment of the interlacing beamlets could, in some situations, lead to the apparition of hot and cold spots in the targeted volume. This has been shown to have limited impact on the target dose for larger, cm-wide proton beams [14], but still has to be studied for smaller beams. This issue will be addressed in a future work.

The radiobiological assumptions, on which grid therapy has been based for over a century, have to be further investigated. The underlying radiobiological processes in grid therapy that promote the protection of the normal tissue are still to be better explained and quantified for additional tissues and beam widths. Eventually, only radiobiological

experiments can reveal which peak doses and VPDRs are tolerated, depending on the beamlet width and c-t-c distance combinations.

Overall, this study showed that by interlacing beamlet arrays incident from opposing directions, a cubic, nearly homogeneous dose distribution could be achieved while maintaining the grid structure of the dose distribution close to the target. This approach can lead to considerable improvements in the normal tissue sparing using grid therapy, also at larger depths in tissue. With this work, we hope to provide guidance for future studies, by both defining the parameters needed as well as providing relevant sets of treatment parameter values and dosimetric values, which can be realized at existing proton therapy centers.

## Disclosure statement

No potential conflict of interest was reported by the authors.

## Funding

Financial support from the Cancer Research Foundations of Radiumhemmet is gratefully acknowledged.

## ORCID

Thomas Henry http://orcid.org/0000-0001-9039-4979

## References

[1] Köhler A. Une nouvelle méthode permettant de faire agir, dans la profondeur des tissus, de hautes doses de rayons Roentgen et un moyen nouveau de protection contre les radiodermites. Ann D'Electrobiologie Radiol. 1909;10:661–664.
[2] Köhler A. Zur Röntgentiefentherapie mit Massendosen. Münchener Medizinische Wochenschrift. 1909;56:2314–2316.
[3] Laissue JA, Blattmann H, Slatkin DN. [Alban Köhler (1874–1947): inventor of grid therapy]. Z Med Phys. 2012;22:90–99.
[4] Laissue JA, Bartzsch S, Blattmann H, et al. Response of the rat spinal cord to X-ray microbeams. Radiother Oncol. 2013;106:106–111.
[5] Mohiuddin M, Fujita M, Regine WF, et al. High-dose spatially-fractionated radiation (GRID): a new paradigm in the management of advanced cancers. Int J Radiat Oncol Biol Phys. 1999;45:721–727.
[6] Zhang X, Penagaricano J, Yan Y, et al. Spatially fractionated radiotherapy (GRID) using helical tomotherapy. J Appl Clin Med Phys. 2016;17:5934.
[7] Zwicker RD, Meigooni A, Mohiuddin M. Therapeutic advantage of grid irradiation for large single fractions. Int J Radiat Oncol Biol Phys. 2004;58:1309–1315.
[8] Bräuer-Krisch E, Serduc R, Siegbahn EA, et al. Effects of pulsed, spatially fractionated, microscopic synchrotron X-ray beams on normal and tumoral brain tissue. Mutat Res. 2010;704:160–166.
[9] Blattmann H, Gebbers JO, Bräuer-Krisch E, et al. Applications of synchrotron X-rays to radiotherapy. Nucl Instr Meth Phys Res Sect A. 2005;548:17–22.
[10] Dilmanian FA, Zhong Z, Bacarian T, et al. Interlaced x-ray microplanar beams: a radiosurgery approach with clinical potential. Proc Natl Acad Sci USA. 2006;103:9709–9714.
[11] Bräuer-Krisch E, Requardt H, Régnard P, et al. New irradiation geometry for microbeam radiation therapy. Phys Med Biol. 2005;50:3103–3111.
[12] Dilmanian FA, Eley JG, Krishnan S. Minibeam therapy with protons and light ions: physical feasibility and potential to reduce radiation side effects and to facilitate hypofractionation. Int J Radiat Oncol Biol Phys. 2015;92:469–474.
[13] Peucelle C, Nauraye C, Patriarca A, et al. Proton minibeam radiation therapy: experimental dosimetry evaluation. Med Phys. 2015;42:7108–7113.
[14] Henry T, Ureba A, Valdman A, et al. Proton grid therapy: a proof-of-concept study. Technol Cancer Res Treat. 2016; DOI: 10.1177/1533034616681670
[15] Lomax AJ, Schaer M. 322 Intensity modulated "grid" proton therapy. Trying to exploit "spatial fractionation" with protons. Radiother Oncol. 2012;102:S171–S173.
[16] Perl J, Shin J, Schumann J, et al. TOPAS: an innovative proton Monte Carlo platform for research and clinical applications. Med Phys. 2012;39:6818–6837.
[17] Grevillot L, Frisson T, Zahra N, et al. Optimization of GEANT4 settings for Proton Pencil Beam Scanning simulations using GATE. Nucl Instr Meth Phys Res Sect B. 2010;268:3295–3305.
[18] Brahme A. Dosimetric precision requirements in radiation therapy. Acta Radiol Oncol. 1984;23:379–391.
[19] Dilmanian FA, Rusek A, Fois GR, et al. Interleaved carbon minibeams: an experimental radiosurgery method with clinical potential. Int J Radiat Oncol Biol Phys. 2012;84:514–519.
[20] Santiago A, Jelen U, Ammazzalorso F, et al. Reproducibility of target coverage in stereotactic spot scanning proton lung irradiation under high frequency jet ventilation. Radiother Oncol. 2013;109:45–50.
[21] Fritz P, Kraus HJ, Mühlnickel W, et al. High-frequency jet ventilation for complete target immobilization and reduction of planning target volume in stereotactic high single-dose irradiation of stage I non–small cell lung cancer and lung metastases. Int J Radiat Oncol Biol Phys. 2010;78:136–142.